Experimental Investigation by Laser Flash Photolysis To Reveal the Optical and Electron-Donating Properties of Benzothiazole Derivatives and a Theoretical Approach by Using Time-Dependent Density Functional Theory

S. K. Pal,[†] T. Sahu (nee Bhattacharya),[†] T. Misra,[†] P. K. Mallick,[‡] M. N. Paddon-Row,[§] and T. Ganguly*,[†]

Department of Spectroscopy, Indian Association for the Cultivation of Science, Jadavpur, Kolkata-700 032, India, Department of Physics, University of Burdwan, Burdwan-713 104, India, and School of Chemistry, University of New South Wales, Sydney, NSW2052, Australia

Received: June 14, 2004; In Final Form: September 8, 2004

The photophysics and electron-donating nature of the three substituted benzothiazoles (BTs) have been studied by electrochemical, steady state, time-resolved spectroscopic techniques. Calculations on isolated molecules in the gas phase as well as solvent environment were performed with use of the density functional theory (DFT) to correlate with the observed polarized spectra. The time-dependent density functional theory (TD-DFT) has been shown to give reasonable singlet and triplet vertical excitation energies for all the BTs studied. The electrochemical measurements demonstrate that the photoinduced electron-transfer (PET) reactions between the donor BT and excited (S_1) acceptor 9-cyanoanthracene (9CNA) are energetically favorable from the thermodynamic point of view. Steady state fluorescence and flash photolysis measurements indicate that the PET is involved only in the excited singlet state of 9CNA in the presence of BTs. It is inferred that the triplet state of 9CNA, being formed by the charge recombination mechanism, would not be involved in the electron-transfer (ET) reaction as the free energy of the triplet state of 9CNA appears to be less than the free energy of the ion-pair (products).

1. Introduction

Photoinduced electron transfer (PET) is one of the most pivotal processes in photosynthesis, photoimaging, optoelectronic, and other microelectronic devices. Investigations on PET processes within the well-defined artificial photosynthetic systems may lead to further insights into the mechanisms of natural photosynthesis. These studies would provide us the information about the first events of the biological processes, which are responsible for a major part of the energy on earth. During the past and in recent years[1−30] PET reactions in linked donor−acceptor model systems, which may mimic the photosynthetic reaction centers in plants, have been found to be of considerable interest. As the photophysics of carbazole donors is well documented in the literature,[31−34] several bichromophoric systems containing carbazole derivatives as donors have been studied.[1] In these systems observations of very fast highly exergonic charge separation (CS) reactions (forward electron transfer) ($k_{CS} \approx 10^{12}$ s^{-1}) coupled with the slower energy wasting charge recombination (CR) (back electron transfer) process ($k_{CR} \approx 10^{8}$ s^{-1}) indicate their behaviors as artificial photosynthetic devices. Further, photoactivity measurements showed that with these systems the efficient photoconducting materials could be developed. Various viologen-linked porphyrins were synthesized and studied by Okura and Hosono[35] to develop suitable redox systems for the photochemical utilization of solar energy. De Schryver et al.[36] studied intramolecular exciplex formation between pyrene and indole moieties. With increasing progress in understanding the elementary process of biological photosynthesis, ET reactions in synthetic porphyrin−quinone systems have found considerable interest.[2,37] Imahori and others[9] observed that in zinc porphyrin−C_{60} dyad the CS rate is about 10^{10} s^{-1} and the energy wasting recombination rate (k_{CR}) is around 10^{6} s^{-1}. Paddon-Row et al.[8] measured the transient absorption spectra of some novel synthesized rigidly bridged dyads and triads by using subpicosecond pump−probe techniques to observe the primary electron-transfer (ET) events. They demonstrated that the primary ET occurs within the triad systems from the donor dimethylaniline to the acceptor dicyanovinyl group, which is connected with the former one by a rigid polynorbornane bridge, within a very short time duration of 10 ps. These systems thus behave as artificial photosynthetic devices. Lately in our laboratory comparative studies[10] were made between intermolecular and intramolecular ET reactions between 4-methoxybenzo[*b*]thiophene (4MBT) donor and *p*-chloroacetophenone (PCA) acceptor by using steady state and laser flash photolysis techniques. The primary aim of our research is to build efficient artificial photosynthetic devices (model donor acceptor linked bichromophoric and multichromophoric systems) where primary charge separation reactions will occur relatively much faster than the energy wasting charge recombination process. It has been shown that the survival duration of charge-separated species before recombination depends on the nature of the linkage, saturated or unsaturated. Although it is well-known that benzothiophenes are potentially useful electron donors, a systematic study of their electron-donating capabilities has not been made. Significant enhancement of the longevity of charge-separated species formed within

* To whom all correspondences should be addressed. E-mail: sptg@mahendra.iacs.res.in/tapcla@rediffmail.com (T. Ganguly). Phone: +91-33-2473-4971, extension 214. Fax: +91-33-2473-2805.
[†] Indian Association for the Cultivation of Science.
[‡] University of Burdwan.
[§] University of New South Wales.

10.1021/jp047445k CCC: $27.50
Published on Web 10/26/2004

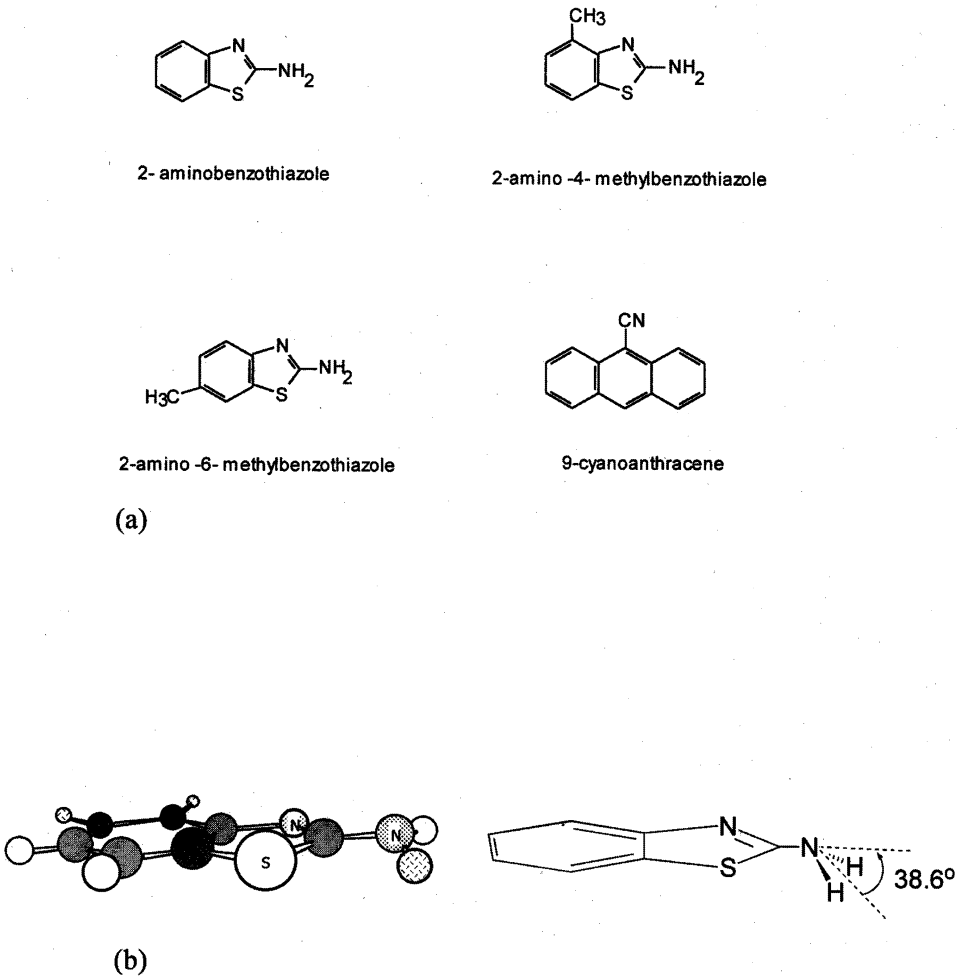

Figure 1. (a) Molecular structures of 2ABT, 2A4MBT, 2A6MBT, and 9CNA. (b) B3LYP/6-31G(d) optimized geometry of 2ABT.

the bichromophore 4MBT/PCA in the presence of β-cyclodextrin (βCD) was recently observed.[38] These studies provide a secure basis for the rational synthesis of efficient organic-based photoconducting materials which might be useful for electrographic/xerographic and microcircuitry industries.

In the present work three substituted benzothiazoles (BTs) have been chosen as electron donors. These are 2-aminobenzothiazole (2ABT), 2-amino-4-methylbenzothiazole (2A4MBT), and 2-amino-6-methylbenzothiazole (2A6MBT) (Figure 1). To our knowledge not much work has been done so far on the photophysical and electron-donating properties of benzothiazoles.[39,40] Apart from the spectroscopic studies, photophysical properties of these donors have been investigated in the present work to reveal the mechanisms of nonradiative processes involved. The electron-donating nature of the present benzothiazoles was examined in the presence of the well-known electron acceptor 9-cyanoanthracene (9CNA)[41] in media of isotropic solvents, e.g., nonpolar *n*-heptane (NH), polar protic ethanol (EtOH), and aprotic acetonitrile (ACN). The results obtained from the intermolecular studies with electrochemical, steady state, and time-resolved spectroscopic techniques are described here. By using time-dependent density functional theory (TD-DFT) vertical excitation energies were computed and correlated with experimental data. It is anticipated that the present studies on intermolecular interactions between the donor benzothiazoles (BTs) and the electron acceptor 9CNA would be helpful for our future studies to assign unambiguously the nature of the intramolecular ET reaction mechanisms within the bichromophores or multichromophoric systems comprising the present benzothiazoles and 9CNA acceptor linked by flexible (polymethylene) and rigid (polynorbornane) bridges.

2. Experimental Section

2.1. Materials. All the samples 2-aminobenzothiazole (2ABT) (97% pure), 2-amino-4-methylbenzothiazole (2A4MBT) (97% pure), 2-amino-6-methylbenzothiazole (2A6MBT) (99% pure), and 9CNA (97% pure), supplied by Aldrich, were purified by vacuum sublimation. The solvents *n*-heptane (NH) (SRL), ethanol (EtOH) (E-Merck), and acetonitrile (ACN) (SRL) of spectroscopic grade were distilled under vacuum according to the standard procedure and tested before use to detect any unwanted impurity emission in the wavelength region studied.

2.2. Spectroscopic Apparatus. At the ambient temperature (296 K) steady-state electronic absorption and fluorescence emission spectra of dilute solutions ($10^{-4}-10^{-6}$ mol dm^{-3}) of the samples were recorded, using 1 cm path length rectangular quartz cells, by means of an absorption spectrophotometer (Shimadzu UV−vis 2101PC) and F-4500 fluorescence spectrophotometer (Hitachi), respectively. Fluorescence lifetimes were measured by using a time-correlated single photon counting (TCSPC) fluorimeter constructed from components purchased from Edinburgh Analytical Instruments (EAI), model 199 UK. The experimental details are given elsewhere.[41] The goodness of fit has been assessed with the help of statistical parameters χ^2 and DW. All the solutions prepared for room temperature measurements were deoxygenated by purging with an argon gas stream for about 30 min.

A special dewar in which a long cylindrical quartz tubing (cell) 3 mm in diameter could be introduced was used for low-temperature (77 K) measurements. The phosphorescence lifetime was measured by using an F-4500 fluorescence spectrophotometer (Hitachi).

The fluorescence quantum yield (ϕ_f) was determined with phenanthrene as standard[42] and the phosphorescence quantum yield (ϕ_p) was measured by using benzophenone as standard.[43] The quantum yield ratio ϕ_p/ϕ_f was computed from the ratio of the area under the corresponding emission curves.[43]

The degree of polarization (P) was measured with the help of UV−vis polarizer accessories including a UV linear dichroic polarizer, wavelength range 230−700 nm, purchased from Oriel Instruments, USA. The observed degree of polarization (P) values were obtained from the following relation.[44]

$$P = [I_{EE} - (I_{BE}/I_{BB})I_{EB}]/[I_{EE} + (I_{BE}/I_{BB})I_{EB}] \qquad (1)$$

Here, I_{EE} and I_{EB} are the intensities of parallel and perpendicular polarized emission with vertically polarized excitation and I_{BB} and I_{BE} are the intensities of horizontally and vertically polarized emission when excited with horizontally polarized light. I_{BE}/I_{BB} defines the instrumental correction factor G (polarization characteristic of the photometric system). This correction is made for any change in the sensitivity of the emission channel for the vertically and horizontally polarized components.

2.3. Laser Flash Photolysis. Transient absorption spectra were measured by using a nanosecond flash photolysis setup (Applied Photophysics) containing an Nd:YAG laser (DCR-11, Spectra Physics). The samples were excited by 355 nm laser light (fwhm = 8 ns). Triplet spectra were monitored through absorption of light from a pulsed Xe lamp (250 W). The photomultiplier (IP28) output was fed into a combiscope (Fluke PM3394B, 200 MHz) and the data were analyzed with Fluke View Combiscope software.

2.4. Electrochemical Measurements. Electrochemical measurements to determine the redox potentials of the reactants were made by using the PAR model 370-4 electrochemistry system. Three electrode systems including SCE as standard were used in the measurements. Tetraethylammonium perchlorate (TEAP) in ACN was used as supporting electrolyte as before.[45]

2.5. Computational Methods. The (gas phase) ground state geometry of 2-aminobenzothiazole (Figure 1) was fully optimized, without symmetry constraints, using the B3LYP hybrid functional[46] and the 6-31G(d) basis set.[47] Gas-phase vertical excitation energies, using the optimized geometries for this molecule, were calculated by using both the semiempirical ZINDO/S method (using the spectroscopic parameter set)[48] and the time-dependent DFT (TD-DFT) method (using the B3LYP hybrid functional and the 6-311+ +G(d,p) basis set).[49] TD-DFT has been shown[50] to give reasonable singlet and triplet vertical excitation energies for a variety of molecules, provided that the states of interest lie well below the ionization threshold, which is the case for the systems discussed here.[51] Thus, the B3LYP/6-311++G(d,p)// B3LYP/6-31G(d,p) lowest vertical ionization potential for 2-aminobenzothiazole is 7.95 eV, whereas the three lowest vertical excitation energies of interest for this molecule lie below 5 eV. The effect of solvation on the computed TD-DFT vertical excitation energies was investigated by using a continuum solvation model, specifically, the polarization continuum model (PCM) implemented for excited states.[52] Because we are interested in vertical excitation energies, the PCM-TD-DFT calculations were carried out with nonequilibrium solvation conditions. It is stressed that, being a continuum solvation model, specific solvent effects, such as solvent−solute H-bonding interactions, are not treated. This may be a problem in the case of ethanol solvent because of the possibility of the presence of solute−solvent H-bonding interaction. The frozen core approximation was used for all TD-DFT calculations; that is, MOs 15 to 270 were used in the correlation. All 46 MOs were used in the ZINDSO/S CI singles calculations. All calculations were carried out with the Gaussian 98 and Gaussian 03 programs.[53,54]

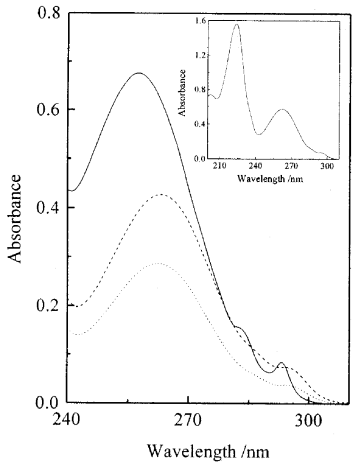

Figure 2. Steady state electronic absorption spectra of 2ABT in NH (the solid line), EtOH (the dashed line), and ACN (the dotted line) at ambient temperature. Inset: Steady state electronic absorption spectra of 2ABT in ACN, showing additionally the 225-nm band.

3. Results and Discussion

3.1. Spectroscopic Properties of BTs. *3.1.1. Electronic Absorption Spectra of BTs.* In solvents of different polarities (NH, EtOH, ACN) the BTs exhibit three main absorption bands at the 225-, 268-, and 292-nm regions (Figure 2). Following the assignments made in the absorption bands of the structurally similar compounds alkoxy benzo[*b*]thiophenes[55] it could be presumed that the longer wavelength band at around 292 nm is due to the $^1L_b \leftarrow {}^1A$ transition and the 268-nm band corresponds to the ^1L_a transition. On the other hand, the whole band system of BTs spanning between 240 and 320 nm undergoes a change in energy (red shift) when the polarity of the medium is increased from NH to EtOH or ACN. Thus, solvent studies indicate the (π,π^*) nature of both the ^1L_a and ^1L_b band systems. Nevertheless, to assign unambiguously the nature of the absorption bands steady-state polarization excitation spectra were measured (vide infra).

3.1.2. Steady-State Fluorescence Emission Spectra of BTs. All the BTs studied in the present investigation were found to be nonfluorescent at ambient temperature irrespective of the polarity of the environment. However, when the temperature is lowered to 77 K, the BTs exhibit a strong phosphorescence spanning between 370 and 540 nm along with a much weaker fluorescence band (Figure 3). The measured phosphorescence decay times of all three BTs, presently studied, in EtOH glassy matrixes were found to be around 135 ms (inset in Figure 3).

The observation of low triplet lifetimes (∼135 ms) coupled with the finding of larger phosphorescence yields relative to fluorescence ($\phi_p/\phi_f \approx 3$) is indicative of formation of BT triplet through the efficient intersystem crossing (isc) process. The internal heavy atom effect[56] due to the presence of sulfur may be responsible for the apparent large ratio of (ϕ_p/ϕ_f) and small lifetime of the lowest triplet state. It is relevant to point out

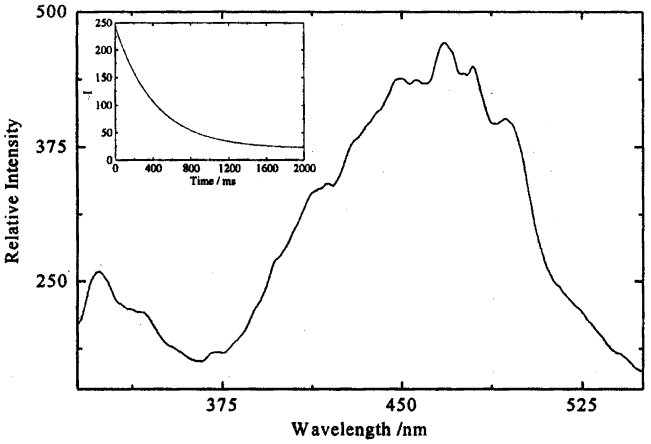

Figure 3. Fluorescence and phosphorescence spectra of 2ABT (concentration $\sim 1.7 \times 10^{-5}$ mol dm^{-3}) in EtOH glassy matrix at 77 K. Inset: The phosphorescence decay of 2ABT ($\lambda_{em} = 467$ nm) in EtOH glassy matrix at 77 K.

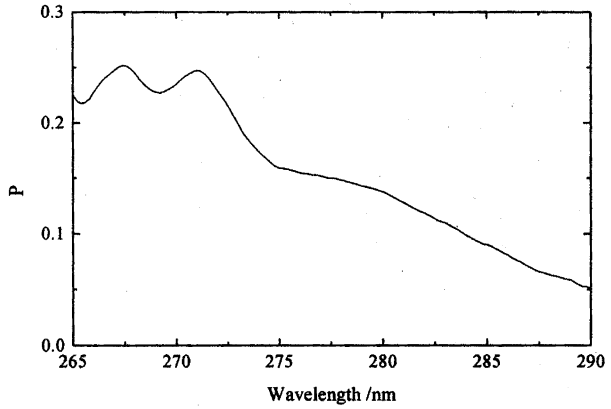

Figure 4. Phosphorescence excitation polarization spectra of 2ABT ($\lambda_{em} = 467$ nm) in EtOH glassy matrix at 77 K.

here that the lack of fluorescence emission of BTs at the ambient temperature may be due to the poorly populated singlet due to the large isc rate, which augments the yield of the triplet state.

3.1.3. Steady-State Phosphorescence Polarization Excitation Spectra at 77 K in EtOH Rigid Glassy Matrix. Figure 4 reproduces the polarized phosphorescence excitation spectra ($\lambda_{em} \approx 397$ nm) for 2ABT in EtOH rigid glassy matrix at 77 K. It can be observed from the figure that the bands in the region of ^1L_a and ^1L_b transitions are positively polarized. This indicates that the $T_1 \leftarrow S_0$ electronic transition should be in near parallel to the transition moments of the two lowest lying singlet electronic states. On the other hand both the ^1L_a and ^1L_b bands corresponding to S_2 and S_1 states situated around the 265 and 290-nm regions, respectively, exhibit significant spectral shift toward the lower energy region (red shift) with the change of polarity of the surrounding solvent (Figure 2), which is in agreement with the (π,π^*) characteristics. The significant different values, though both positive, of the degree of polarization at 265 and 290 nm indicate that these bands correspond to two different transitions. Moreover toward the 290-nm region, *P* values decrease considerably showing a somewhat depolarization effect in this ^1L_b region.

The angles (α) between the absorption and emission transition dipole moment were calculated by using the experimentally measured degree of polarization (*P*) value with the following equation:

$$P = [3\cos^2\alpha - 1]/[\cos^2\alpha + 1] \quad (2)$$

The values of α obtained from eq 2 were 39° for the 265-nm band and 52° for the 290-nm band. From these values the angle between the transition dipole moments of the 265- and 290-nm bands was computed and was found to be ~13°. Such a small value of the angle between the transition moments of ^1L_a and ^1L_b bands indicates that there is a possibility of mixing between the two lowest excited singlet states, S_1 and S_2. As the ^1L_b band is weak it might contain intensity-borrowing from the higher electronic state ^1L_a.[57] The mixing of S_1 and S_2 states may facilitate intensity-borrowing and the ^1L_b band may acquire some characteristics of the ^1L_a transition. It makes the transition dipole moment of the ^1L_b band closer to that of ^1L_a. Due to the contamination of the ^1L_a state in the region of ^1L_b large depolarization might occur in this region, which was actually observed in the phosphorescence polarization excitation spectra (Figure 4) from very low *P* values.

3.2. Ground-State Calculations. *3.2.1. Molecular Geometry and Ground-State Dipole Moment.* The B3LYP/6-31G(d) optimized ground-state geometries of 2-aminobenzothiazole are shown in Figure 1b (Cartesian coordinates are provided in the Supporting Information). With the exception of the two NH_2 hydrogen atoms, the remaining atoms lie in a plane with an rms deviation of 0.013°. The exocyclic amino nitrogen is pyramidalized, the out-of-plane flap angle being 38.6°. The ground-state dipole moment is predicted to be 2.04 D.

3.2.2. Excited States. Vertical excitation energies and oscillator strengths calculated in the gas phase with TD-DFT at the B3LYP/6-311++G(d,p)//B3LYP/6-31G(d) level of theory are listed in Table 1, along with experimental values (oscillator strengths were measured from absorption spectra by using the equation $f = 4.32 \times 10^{-9} \int \epsilon(\bar{\nu})\, d\bar{\nu}$[58]). Type of transitions ((π,π^*) or (n,π^*)) deduced by graphical visualization of the molecular orbitals shows that first and third singlet states are of (π,π^*) nature. TD-DFT simulated oscillator strength of the third singlet state is somehow larger than that of the first singlet state. From the above observations the first and the third singlet states may be assigned as ^1L_b and ^1L_a transitions, respectively. Thus, this method correctly predicts two low-lying (π,π^*) electronic transitions: a ^1L_a and a ^1L_b. The ^1L_b transition is lower in energy, followed by the ^1L_a transition. Orbital configurations of ^1L_b and ^1L_a states show that these states share HOMO → LUMO+1, HOMO → LUMO+2 and HOMO → LUMO+3 transitions. This is in agreement with the possibility of mixing of the states ^1L_b (S_1) and ^1L_a (S_2), which is apparent from the experiment. In the gas phase the TD-DFT method yielded transition energies all within 0.5 eV of experiment and that correlate well with the experimental data. TD-DFT predicts the ^1L_b oscillator strength with good agreement with the experimental data but the method is less accurate for calculating the ^1L_a oscillator strength of 2ABT in the gas phase.

The transition energies and oscillator strengths of 2ABT in the gas phase predicted by the ZINDO/S//B3LYP/6-31G(d) level of theory are listed in Table 2 along with experimental values. Though the vertical excitation energies of the first and third singlet states are very similar to the experimental values it is difficult to assign these states as ^1L_b and ^1L_a transitions respectively due to the lack of similarities of the oscillator strengths of these states with the experimental values and the (n,π^*) nature of the third singlet state. So, it is clear that ZINDO/S provides less satisfactory results for the excited states of 2ABT than the TD-DFT method. The simulated in vacuo line spectra of 2ABT, calculated by using the above two

TABLE 1: Time-Dependent DFT Simulation of Vertical Excitation Energies and Oscillator Strengths of 2-Aminobenzothiazole at the B3LYP/6-311++G(d,p)//B3LYP/6-31G(d) Level of Theory

	energy (eV)			oscillator strength, au	
transition type	gas phase	EtOH (exptl)[a]	energy shift, cm^{-1}	gas phase	EtOH (exptl)[a]
$(\pi,\pi^*)^1$ ($^1L_b \leftarrow {}^1A$)	4.58	4.68 (4.20)	817.3	0.0105	0.0154 (0.0081)
$(\pi,\pi^*)^1$	4.69	4.79	779.8	0.0022	0.0366
$(\pi,\pi^*)^1$ ($^1L_a \leftarrow {}^1A$)	4.91	4.87 (4.70)	−334.8	0.1446	0.2398 (0.2960)
$(\pi,\pi^*)^1$	4.99	5.23	1846.2	0.0041	0.0052
$(\pi,\pi^*)^1$	5.02	5.28	2081.6	0.0399	0.0006
$(\pi,\pi^*)^1$	5.42	5.40	−171.0	0.0994	0.1775
$(\pi,\pi^*)^3$	3.36	3.36 (3.00)	0.0	0.0000	0.0000
$(n,\pi^*)^{3\,b}$	5.51	5.51	0.0	0.0000	0.0000

[a] Experimental values were measured in ethanol (EtOH) solvent. [b] 10th triplet excited state.

TABLE 2: Simulation of Vertical Excitation Energies and Oscillator Strengths of 2-Aminobenzothiazole at the ZINDO/S//B3LYP/6-31G(d) Level of Theory[a]

		CI	gas phase (exptl)[d]	
transition type	orbitals	expansion coeff	energy, eV	oscillator strength, au
$(\pi,\pi^*)^1$	24→26[c]	−0.227	4.25 (4.20)	0.2665 (0.0081)
	25[b]→26	0.592		
	25→27	−0.224		
$(\pi,\pi^*)^1$	24→26	0.302	4.28	0.00721
	25→26	0.322		
	25→27	0.513		
$(n,\pi^*)^1$	23→26	0.606	4.75 (4.70)	0.0074 (0.2960)
	23→28	0.340		
$(\pi,\pi^*)^1$	24→26	−0.207	5.29	0.0074 (0.2960
	24→27	0.388		
	25→28	0.518		
$(\pi,\pi^*)^1$	24→26	0.521	5.48	0.7257
	24→27	0.229		
	25→27	−0.353		
$(\pi,\pi^*)^3$	24→27	−0.363	1.95 (3.00)	0.0000
	25→26	0.519		
$(n,\pi^*)^{3\,e}$	25→29	0.565	5.43	0.0000
	26→30	0.228		

[a] Only CI expansion coefficients with absolute vales >0.2 are included in the table. [b] HOMO. [c] LUMO. [d] Experimental values were measured in ethanol (EtOH) solvent. [e] 10th triplet excited state.

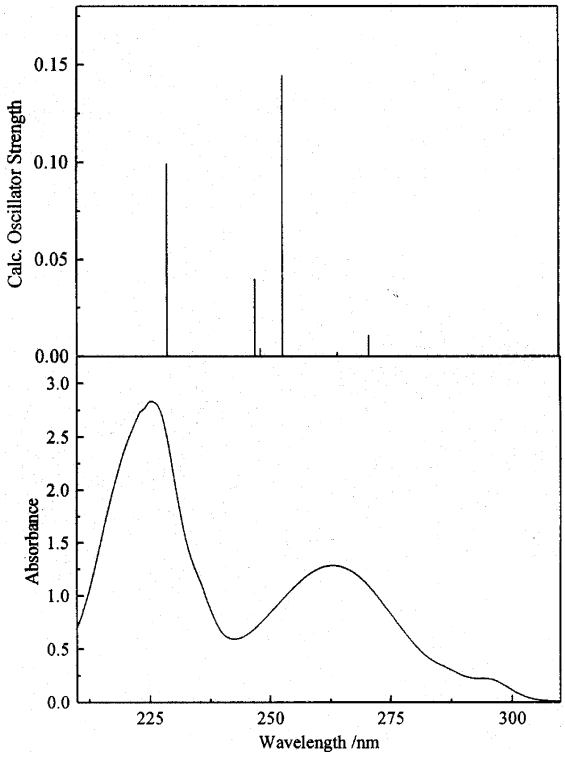

Figure 5. UV−vis absorption spectra of 2ABT in EtOH. The UV−vis line spectrum calculated for 2ABT in vacuo by TD-DFT calculation is shown in the top section of the figure.

methods, are shown in Figures 5 and 6, and the properties of the calculated spectra are shown in Tables 1 and 2.

The TD-DFT method predicted appreciable shift in energy for singlet states in going from the gas phase to the solvent phase (Table 1). The effects of various solvents (ACN, EtOH, and NH) on calculated vertical excitation energies and oscillator strengths with use of TD-DFT are listed in Table 3. There are no appreciable shifts of vertical excitation energies on going from ACN to EtOH, which was apparent from the experimental results. Moreover, on going from NH to ACN no significant spectral shift of the vertical excitation energies is observed though experimentally there was a red shift. Due to introduction of solvent effect the TD-DFT method becomes more accurate in predicting ^1L_a oscillator strength too.

TD-DFT predicted (both in the gas phase and in the solvent phase) the (π,π^*) nature of the both the lowest singlet and triplet excited states of 2ABT. This method also showed that both the $(\sigma,\pi^*)^3$ and $(n,\pi^*)^3$ states are significantly higher in energy, by more than 1 eV, than the lowest energy (π,π^*) excited singlet state. So, the spin−orbit coupling between $(\pi,\pi^*)^1$ with either the $(\sigma,\pi^*)^3$ or $(n,\pi^*)^3$ states should be small. In contrast, there is a $(\pi,\sigma^*)^3$ state that is only slightly lower in energy than the first excited singlet state (in heptane, ethanol, and acetonitrile solvents, the $(\pi,\sigma^*)^3$ triplet lies respectively only 0.14, 0.06, and 0.05 eV below that of the first excited singlet state). Moreover, inspection of the active σ^* molecular orbital in the $(\pi,\sigma^*)^3$ configuration reveals it to be localized to the sulfur atom and its two nearest neighboring carbon atoms. These two factors, namely the very small energy gap between the $(\pi,\sigma^*)^3$ and the first $(\pi,\pi^*)^1$ states and the significant contribution of sulfur atomic orbitals to the $(\pi,\sigma^*)^3$ state (the heavy atom effect[59]), ensure a strong spin−orbit coupling between these two states and a consequent rapid isc passage from the $(\pi,\pi^*)^1$ state to the $(\pi,\sigma^*)^3$ state, followed by rapid and irreversible internal conversion to the lowest energy triplet state, $(\pi,\pi^*)^3$.

3.2.3. Transition Dipoles. The TD-DFT transition dipoles of 2ABT in the gas phase for the ^1L_b and ^1L_a transitions possess out-of-plane contributions of 0.0101 and 0.0001 au, respectively. The $\pi-\pi^*$ transitions for planar aromatics are the result of electronic transitions between π and π^* orbitals that are strictly symmetric with respect to the molecular plane and, consequently, there would be no out-of-plane component associated

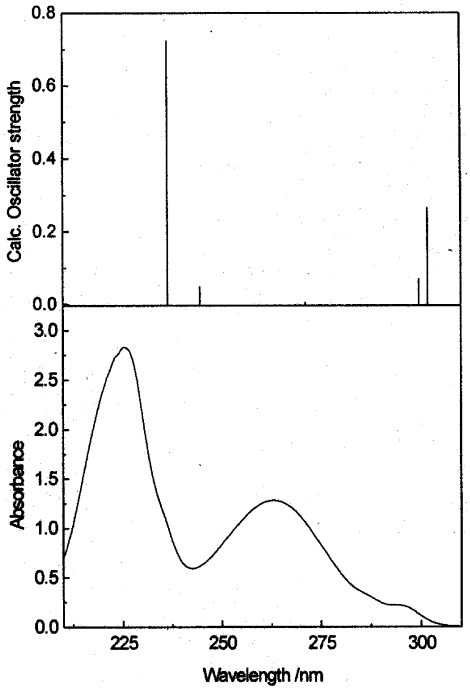

Figure 6. UV−vis absorption spectra of 2ABT in EtOH. The UV−vis line spectrum calculated for 2ABT in vacuo by ZINDO/S calculation is shown in the top section of the figure.

TABLE 3: Time-Dependent DFT Simulation of Vertical Excitation Energies and Oscillator Strengths of 2-Aminobenzothiazole in Various Solvents at the B3LYP/6-311++G(d,p)//B3LYP/6-31G(d) Level of Theory

	energy, eV			oscillator strength, au		
transition type	ACN (exptl)[a]	EtOH (exptl)[a]	NH (exptl)[a]	ACN (exptl)[a]	EtOH (exptl)[a]	NH (exptl)[a]
$(\pi,\pi^*)^1$	4.68	4.68	4.66	0.0151	0.0154	0.0206
$(^1L_b \leftarrow {}^1A)$	(4.20)	(4.20)	(4.25)	(0.0085)	(0.0081)	(0.0098)
$(\pi,\pi^*)^1$	4.80	4.79	4.69	0.0384	0.0366	0.0064
$(\pi,\pi^*)^1$	4.87	4.87	4.86	0.2345	0.2398	0.2668
$(^1L_a \leftarrow {}^1A)$	(4.70)	(4.70)	(4.80)	(0.2966)	(0.2960)	(0.3010)
$(\pi,\pi^*)^1$	5.23	5.23	5.08	0.0051	0.0052	0.0045

[a] Experimental values were measured in corresponding solvent.

with the transition dipoles. However, the planarity of 2ABT is destroyed, by the pyramidalization of the amino nitrogen atom. This nonplanarity is probably the source of the small out-of-plane contributions to that predicted for the ^1L_b and ^1L_a transitions.

The TD-DFT-calculated angle in the gas phase between the ^1L_a and ^1L_b transition dipoles of 2ABT is 19°. Such a small angle between ^1L_a and ^1L_b was also apparent from the polarization experimental data, as discussed above. From the experimentally observed P values, the angle between the transition dipole moments of ^1L_a and ^1L_b was estimated to be ∼13°. However, the solvent (EtOH) effect in the TD-DFT calculations yielded a value of 16°, which is in better agreement with experiment.

3.3. Possibility of Photoinduced Electron Transfer (PET) within the Present Donor Acceptor Systems. *3.3.1. Electrochemical Studies.* With use of cyclic voltammetry (details are given in the Experimental Section) the redox potentials of benzothiazoles (2ABT/2A4MBT/2A6MBT) and 9CNA in ACN fluid solution were measured. The half-wave reduction potential, $E_{1/2}^{RED}(A^-/A)$, of 9CNA was found to be −1.13 eV. On the other hand due to the irreversibility of the reaction shown in electrochemical measurements, half-wave oxidation potentials,

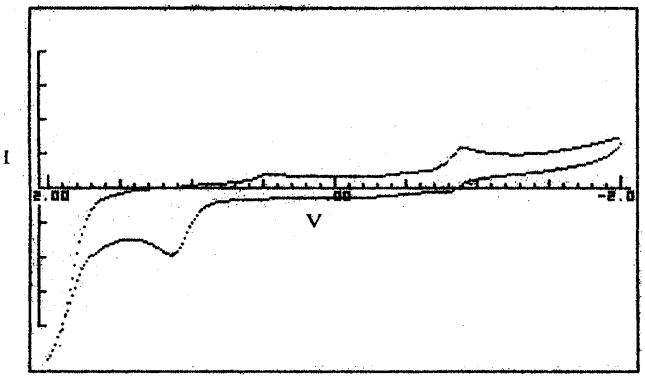

Figure 7. $I-V$ curve of 2ABT in ACN obtained in cyclic voltammetry measurement.

$E_{1/2}^{OX}(D/D^+)$, of the BTs could not be determined accurately. However, from the $I-V$ curve shown in Figure 7, as an approximation the half-wave oxidation potential values of the BTs are chosen as +1.2 eV. With use of the well-known Rehm−Weller relation[1] (eq 3), the free energy change, ΔG_{ET}^0, associated with radical ion-pair formation could be computed,

$$\Delta G_{ET}^0 = E_{1/2}^{OX}(D/D^+) - E_{1/2}^{RED}(A^-/A) - E_{0,0}^* - e^2/4\pi\epsilon_0\epsilon_s R \quad (3)$$

$E_{0,0}^*$ is the first singlet−singlet transition energy ((0,0) band) of the acceptor and the fourth term represents the Coulomb stabilization term whose contribution to the value of ΔG_{ET}^0 is negligible (∼0.06 eV) in highly polar solvent ACN. From eq 2, the ΔG_{ET}^0 value was computed for the present BT-9CNA* (the asterisk denotes the excited singlet state) systems in ACN fluid solution. This was found to be ca. −0.8 eV ($E_{0,0}^* \approx 3.08$ eV).[55] Thus, the PET reactions within the ground state donor BT and exited (S_1) acceptor 9CNA are energetically favorable from the thermodynamic point of view and fall in the intermediate region (0.4 eV $\leftarrow \Delta G_{ET}^0 <$ 2.0 eV)[60] where the bimolecular quenching reactions due to ET should proceed through diffusion-controlled mechanisms. The studies made on the quenching phenomena observed in the fluorescence emission of 9CNA in the presence of BTs are described below.

3.3.2. Spectroscopic Investigation. Steady-state fluorescence intensity of 9CNA has been observed to be quenched throughout its entire band envelope in the presence of the BTs (Figure 8). The steady-state fluorescence quenching data have been analyzed following Stern−Volmer (SV) equation

$$\frac{f_0}{f} = 1 + k_q\tau_0[Q] \quad (4)$$

where f_0 and f are fluorescence intensities of the fluorophore 9CNA in the absence and presence of the quencher, k_q is the bimolecular quenching rate constant, [Q] is the concentration of the quencher, $K_{SV} = k_q\tau_0$ is the Stern−Volmer quenching constant, and τ_0 is the acceptor fluorescence lifetime in the absence of quencher, which is measured experimentally by using time correlated single photon counting (TCSPC) technique whose details are given in the Experimental Section. It is important to point out here that as the fluorescence quenching of 9CNA occurs in the region of BT concentrations where the 9CNA absorption spectrum is not at all affected, the simple SV equation was used to analyze the quenching phenomena.

In both polar solvents EtOH and ACN the linearity in the SV plot (inset of Figure 8a) was obtained over the entire range

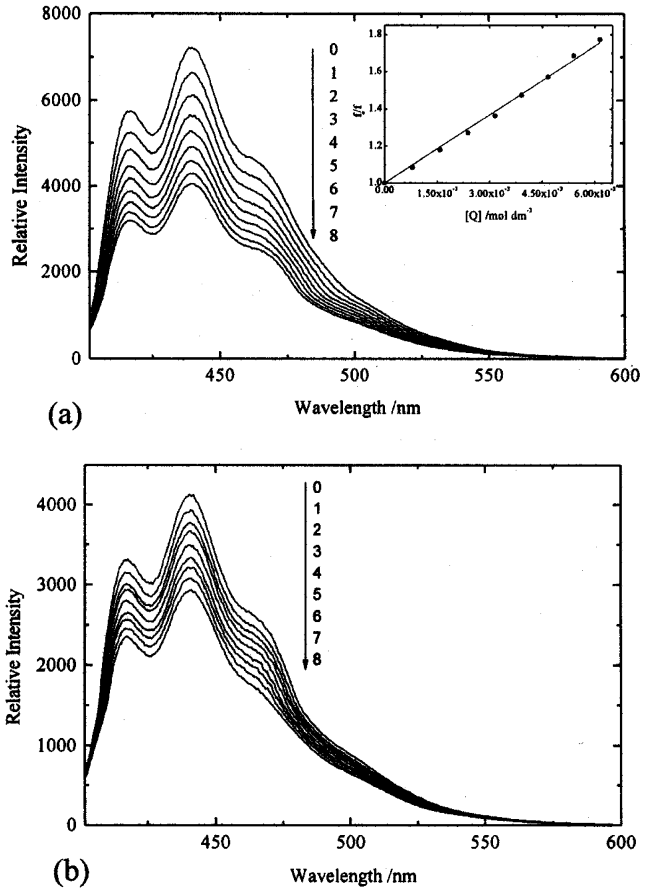

Figure 8. (a) Fluorescence emission spectra of 9CNA (concentration $\sim 2.0 \times 10^{-5}$ mol dm^{-3}) ($\lambda_{ex} = 402$ nm) in ACN at 296 K in the presence of 2ABT: (0) 0, (1) 8.1×10^{-4}, (2) 1.6×10^{-3}, (3) 2.4×10^{-3}, (4) 3.2×10^{-3}, (5) 3.9×10^{-3}, (6) 4.7×10^{-3}, (7) 5.4×10^{-3}, (8) 6.1×10^{-3} mol dm^{-3}. Inset: Stern−Volmer (SV) plot from steady-state fluorescence emission intensity measurements in the case of singlet (S_1) excitation of 9CNA in the presence of 2ABT in ACN fluid solution at 296 K. (b) Fluorescence emission spectra of 9CNA (concentration $\sim 2.0 \times 10^{-5}$ mol dm^{-3}) ($\lambda_{ex} = 402$ nm) in EtOH at 296 K in the presence of 2ABT: (0) 0, (1) 8.1×10^{-4}, (2) 1.6×10^{-3}, (3) 2.4×10^{-3}, (4) 3.2×10^{-3}, (5) 3.9×10^{-3}, (6) 4.7×10^{-3}, (7) 5.4×10^{-3}, (8) 6.1×10^{-3} mol dm^{-3}.

of the quencher concentrations. This indicates a favoring of the occurrence of dynamic quenching of fluorescence emission of 9CNA in the presence of BTs. Moreover, the τ_0/τ value (τ is the quenched fluorescence lifetime of 9CNA in the presence of donors which act as quenchers) was found to be equal to f_0/f. This further confirms the dynamic nature of the quenching phenomena.

The values of K_{SV} and k_q of 2ABT + 9CNA* (the asterisk indicates excited electronic state S1), 2A4MBT + 9CNA*, and 2A6MBT + 9CNA* in both ACN and EtOH solvents are shown in Table 4.

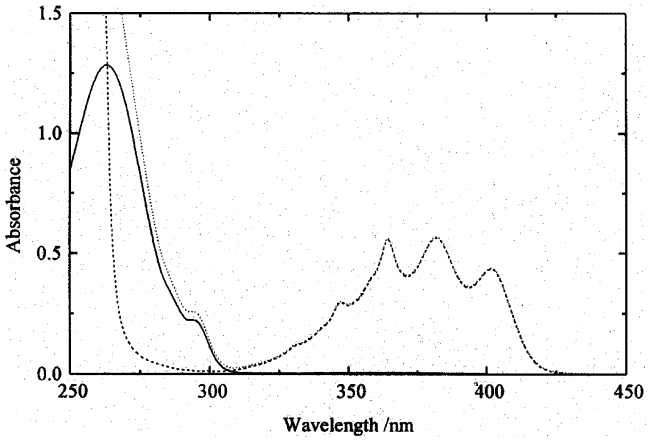

Figure 9. Electronic absorption spectra of 2ABT (concentration $\sim 8.7 \times 10^{-5}$ mol dm^{-3}, the solid line), 9CNA (concentration $\sim 8.1 \times 10^{-5}$ mol dm^{-3}, the dashed line), and a mixture (the dotted line) of 2ABT (concentration $\sim 8.7 \times 10^{-5}$ mol dm^{-3}) and 9CNA (concentration $\sim 8.1 \times 10^{-5}$ mol dm^{-3}) in EtOH fluid solution at 296 K, $l = 1$ cm.

The k_q values are found to be close to the diffusion controlled rates, k_d ($=8RT/3000\eta$),[61] in EtOH solvent and in ACN medium these values are not very different from k_d. This observation is in accord with our expectation as Kikuchi[60] pointed out that when ΔG^0_{ET} values fall in the intermediate region (for the present donor−acceptor systems, the $-\Delta G^0_{ET}$ value was found to be $\sim$0.8 eV) the value of k_q should be close to k_d if the fluorescence quenching occurs primarily due to photoinduced electron-transfer reactions. Nevertheless, in the present investigations attempts were made to search whether some other, apart from PET, nonradiative processes are present. The results obtained from the detailed investigations are described below.

As no ground-state complex formation was apparent from the steady-state absorption measurements of the mixture of a BT and 9CNA, having similar concentrations as used in the quenching studies, the possibility of the presence of the static mode in the observed fluorescence quenching of 9CNA should be ignored. Again, as at the excitation wavelength ($\sim$402 nm) BTs are completely transparent (Figure 9), the chance of the competitive absorption by BT as well as the inner filter effect to the fluorescence emission of 9CNA has been ruled out. Moreover, as in the present case the acceptor 9CNA was excited, the possibility of nonradiative energy transfer as a source of quenching should be excluded.

3.3.3. Transient Optical Absorption Measurements. To obtain the direct evidence of the occurrence of photoinduced electron-transfer reactions within the present donor−acceptor systems in ACN and EtOH solvents the transient optical absorption spectra were recorded at the end of a 8-ns flash. To avoid the possibility of interference in the energy transfer process the third harmonic (355 nm) of the Nd:YAG laser was used to excite

TABLE 4: Fluorescence Quenching Data for the Present D−A Systems at 296 K, * Denotes Excited Singlet State

system	K_{SV}, dm^3 mol^{-1}	τ_0, ns ($\pm$0.4)	$k_q \times 10^{10}$, dm^3 mol^{-1} s^{-1}	$k_d^b \times 10^{10}$,[b] dm^3 mol^{-1} s^{-1}
2ABT + 9CNA* + ACN	123.1	16.1	0.76	$\sim$1.90
2ABT + 9CNA*+EtOH	62.79	15.6	0.40	$\sim$0.61
2A4MBT + 9CNA* + ACN	384.92	16.1	2.24	$\sim$1.90
2A4MBT + 9CNA* + EtOH	172.32	15.6	1.10	$\sim$0.61
2A6MBT + 9CNA* + ACN	174.75	16.1	1.02	$\sim$1.90
2A6MBT + 9CNA* + EtOH	109.13	15.6	0.70	$\sim$0.61

[a] The asterisk (*) denotes the excited singlet state. τ_0 denotes the acceptor fluorescence lifetime in the absence of quencher. [b] Values of k_d obtained[61] using the relation $k_d = (8RT/3000\eta)$.

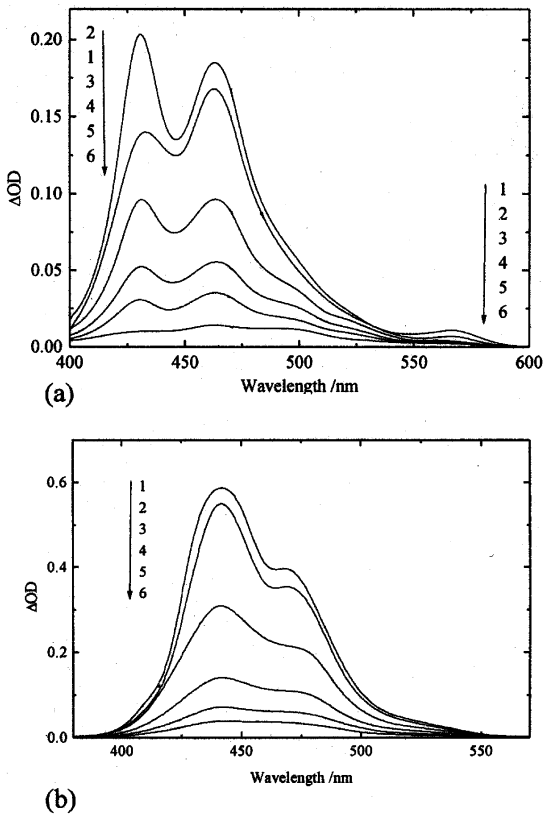

Figure 10. (a) Transient absorption spectra of the mixture of 9CNA and 2ABT (excitation wavelength ~355 nm) at the ambient temperature at the following delay times: (1) 1.0, (2) 1.5, (3) 2.0, (4) 2.5, (5) 3.0, and (6) 3.5 μs measured in ACN. (b) Transient absorption spectra of the mixture of 9CNA and 2ABT (excitation wavelength ~355 nm) at the ambient temperature at the following delay times: (1) 1.0, (2) 1.2, (3) 1.5, (4) 2.0, (5) 2.5, and (6) 3.0 μs measured in EtOH.

specifically the acceptor 9CNA from the mixture of the acceptor 9CNA and benzothiazole donors.

The transient absorption spectra of 9CNA was measured in the presence of 2ABT in both ACN and EtOH. A broad band peaking at ~430 nm was observed in ACN solvent (Figure 10a). The kinetics of the absorption decay at 430 nm demonstrate that the decay is of biexponential nature. The shorter component ($\tau_1 \approx 1$ μs) corresponds to the lifetime of the cationic species of 9CNA and the value of the longer one is 560 μs, the triplet lifetime of the monomeric 9CNA.[55] Moreover, the fractional contribution (*f*) of the shorter component is 0.01 whereas that of the longer one is 0.99. Thus, the 430-nm band is mostly due to the monomeric triplet of 9CNA. According to Zimmermann et al.[62] the absorption band of the radical cation of 9CNA resides energetically very close (large overlapping) to the corresponding band of pure (monomer) 9CNA, whose triplet lifetime is ~560 μs. From the thermodynamical considerations Zimmermann[62] inferred that the formation of the cationic species of 9CNA due to electron transfer from singlet excited 9CNA to the solvent ACN is more favorable than the formation of the radical anion by capturing an electron from the solvent. This proposition is quite in agreement with the experimentally observed decay (~1 μs) at 430 nm.

In addition to 430-nm band, another band peaking at ~460 nm was observed in the transient spectra of the mixture of 9CNA and 2ABT in ACN. The decay profile at 460 nm was fitted to a single-exponential analysis and the lifetime was determined to be 1.0 μs under argon. This transient was quenched by oxygen with a rate constant of 1/9th of the diffusion-controlled

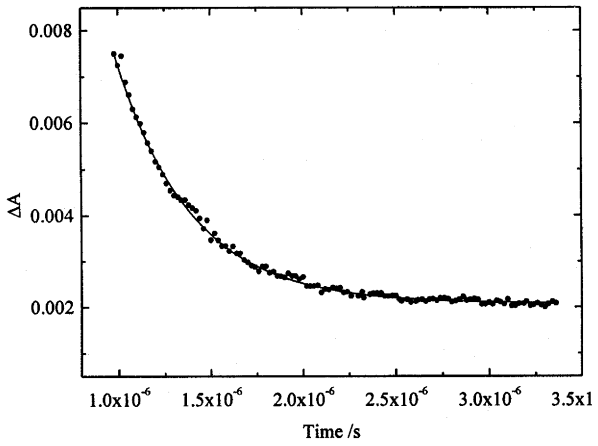

Figure 11. The time profile of the absorbance (ΔA) of the acceptor 9CNA radical anion in the presence of 2ABT in ACN at 570 nm.

quenching rate constant. On the basis of these observations and the earlier report,[63] the observed transition can be assigned to the triplet state of 2ABT.

Following the earlier report,[62] the broad spectrum observed around 570 nm in ACN solvent could be assigned to the band of the 9CNA radical anion ($9CNA^-$) of the contact ion-pair. This observation clearly demonstrates that photoinduced ET reactions within the present donor acceptor systems take place leading to the formation of the radical ion-pair.

The time profile of the absorbance of the acceptor 9CNA anion in ACN at 570 nm is reproduced in Figure 11. The absorption decay is represented by a single exponential with an ion-pair lifetime (τ_{ip}) defined as in eqs 5 and 6, of the order of 0.4 μs,

$$\tau_{ip} = (k_{cr} + k_{dis})^{-1} \quad (5)$$

$$\phi_R = k_{dis}\tau_{ip} \quad (6)$$

where k_{cr} and k_{dis} represent the rates associated with the geminate recombination and charge dissociation (solvent separated ion-pair formation) processes, respectively. The yield ϕ_R of dissociated ion radical formations is obtained by taking the ratio of the constant absorbance at long delay times due to dissociated ions and the initial value estimated by extrapolating the ion absorbance to $t = 0$ in Figure 11. The value of ϕ_R is ~0.03, which is low enough, and the value of k_{cr} is found to be significantly larger than that of k_{dis} ($k_{cr} \sim 2.4 \times 10^6$ s^{-1}, $k_{dis} \approx 6.3 \times 10^4$ s^{-1}). Such a large value of the charge recombination rate compared to the rate of the charge dissociation indicates the formation of CIP of tight nature, which results in very poor charge dissociation yield.

One could see from the transient absorption spectra of 9CNA in the presence of 2ABT in ACN that with the increase of delay times from 1.0 μs to 4.0 μs, the anionic band decreases following the geminate charge recombination process. On the other hand monomeric triplet bands of both acceptor (430 nm in ACN) and donor (460 nm in ACN) display different time-dependent behavior. With gradual increase in delay these bands were found to be enhanced accompanied by the concurrent reduction of absorbance of the radical anion of 9CNA. It appears that buildup of the monomeric triplet of both acceptor 9CNA and donor 2ABT occurs in the same time interval during which the radical anionic species of 9CNA disappears. This infers that the production of the monomeric triplet of both donor and acceptor occurs through the ion recombination mechanism. Nevertheless,

SCHEME 1[a]

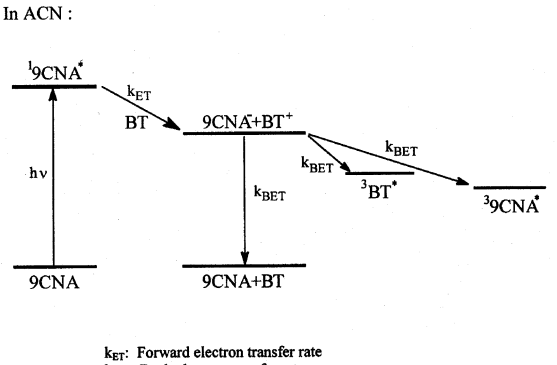

k_{ET}: Forward electron transfer rate
k_{BET}: Back electron transfer rate
The subscripts 1 and 3 represent the singlet and triplet state respectively.
* represents the excited state.

[a] In EtOH, the ion-pair ($9CNA^- + BT^+$) recombination rate seems to be much faster than the time resolution of the instrument (no ions could be detected but ^{3}BT* is clearly apparent).

as the donor contains heavy atom sulfur (S), its presence may also additionally help in building up the triplet of the acceptor through the external heavy atom effect.[56]

Figure 10b reproduces the transient absorption spectra of 9CNA in the presence of the donor 2ABT in EtOH solvent. The broad band at about 440 nm may be assigned as the monomeric triplet of 9CNA. No direct evidence of occurrence of electron transfer within the present donor acceptor systems is apparent from the figure as the anionic or cationic band is totally absent in this transient spectra. The only indirect evidence is the presence of the monomeric triplet band of donor 2ABT (~477 nm), which can be formed only through the charge recombination mechanism. Though electron-transfer reaction may take place in the above donor−acceptor system in EtOH there is no ionic ($9CNA^-$ or $2ABT^+$) band in the transient spectra. It seemingly indicates that in the EtOH solvent the charge recombination process is very fast and the ion-pair lifetime is smaller than the response of our laser flash photolysis system.

From all the above observations, we conclude that the photoinduced electron transfer is involved in the singlet state of 9CNA in the presence of BTs. As there is no quenching observed in the triplet lifetime of 9CNA (~560 μs) in the presence of BT, it could be inferred that the triplet state after forming by the charge recombination mechanism would not be involved in ET reactions. This finding is in accord with our expectation as the free energy of the triplet state of 9CNA should be less than the free energy of the ion-pair. The phenomena of excited-state dynamics observed from the present investigation have been depicted in the Scheme 1.

From above discussion it is apparent that oxidation potentials of the donors are nearly equal and the quenching rate k_q remains nearly unchanged irrespective of the surrounding solvents. The photophysical properties of all BTs are also nearly the same. So we can conclude that the substitution effects do not significantly affect our systems.

4. Conclusions

In the present investigation new results associated with the photophysical and electron-donating properties of some benzothiazoles (BTs) have been provided. The steady-state polarization measurements coupled with the computed values of transition energies of BTs predicted by the B3LYP/6-311++G(d,p) level of theory show that a very small angle (~16°) exists between the two lowest lying excited electronic states, ^1L_a and ^1L_b. This small angle seems to be responsible for the mixing of these two lowest lying excited states S_1 and S_2. Moreover, ^1L_b (S_1) being much weaker might contain intensity borrowed from the higher electronic state ^1L_a(S_2) making the transition dipole moment of the former closer to that of the latter. It was demonstrated from the electrochemical measurements along with laser flash photolysis studies that BTs undergo photoinduced ET reactions with excited 9CNA in the intermediate region and form CIP of tighter nature due to the charge recombination process becoming dominant over charge dissociation. It is also inferred that though the PET reactions occur in the excited singlet of 9CNA, its triplet after formation by the charge recombination mechanism would not be involved in ET reactions.

Acknowledgment. The authors are grateful to the Department of Inorganic Chemistry for electrochemical measurements. Thanks also are due to the Department of Organic Chemistry for helping in purification of the samples. We wish to express our heartiest thanks to Prof. Samita Basu and Ms Sharmistha Dutta Choudhury of the Saha Institute of Nuclear Physics, Kolkata, for helping in the measurements of the transient absorption spectra by laser flash photolysis technique. T.B. acknowledges the financial support provided by the Council of Scientific and Industrial Research (CSIR), New Delhi, India in the form of grants and fellowships. Paddon-Row thanks the Australian Research Council for support and the Australian Partnership for Advanced Computing and the Australian Centre for Advanced Computing and Communications for allocation of computing time.

Supporting Information Available: B3LYP/6-31G(d) optimized geometry of 2-amino-benzothiazole in the gas phase. This material is available free of charge via the Internet at http://pubs.acs.org.

References and Notes

(1) Ganguly, T.; Sharma, D. K.; Gauthier, S.; Gravel, D.; Durocher, G. *J. Phys. Chem.* **1992**, *96*, 3757.
(2) Staab, H. A.; Weiser, J.; Baumann, E. *Chem. Ber.* **1992**, *125*, 2275.
(3) De Schryver, F. C.; Declereq, D.; Depaemelaere, S.; Hermans, E.; Onkelinx, A.; Verhoeven, J. W. *J. Photochem. Photobiol. A: Chem.* **1994**, *82*, 171.
(4) Vandijk, S. I.; Groen, C. P.; Hartel, F.; Brouwer, A. M.; Verhoeven, J. W. *J. Am. Chem. Soc.* **1996**, *118*, 8425.
(5) Yoshimura, A.; Nozaki, K.; Ikeda, N.; Ohno, T. *J. Phys. Chem.* **1996**, *100*, 1630.
(6) de Silva, A. P.; Gunaratne, H. Q. N.; Gunnlaugsson, T.; Huxley, A. J. M.; McCoy, C. P.; Rademacher, J. T.; Rice. T. E. *Chem. Rev.* **1997**, *97*, 1515.
(7) Fukuzumi, S.; Imahori, H.; Yamada, H.; El-Khowly, M. E.; Fujitsuka, M.; Ito, O.; Guldi, D. M. *J. Am. Chem. Soc.* **2001**, *123*, 2571.
(8) Seischal, M.; Lodenkemper, T.; Stockmann, A.; Schmeider, S.; Koeberg, M.; Roest, M. R.; Verhoever, J. W.; Lawson, J. M.; Paddon-Row, M. N. *Phys. Chem. Chem. Phys.* **2000**, *2*, 1889.
(9) Imahori, H.; El-Khouly, M. E.; Fijitsuka, M.; Ito, O.; Sakata, Y.; Fukuzumi, S. *J. Phys. Chem. A* **2001**, *105*, 325.
(10) Maiti, M.; Misra, T.; Bhattacharya, T.; Basu, C.; De, A.; Sarkar, S. K.; Ganguly, T. *J. Photochem. Photobiol. A: Chem.* **2002**, *152*, 41.
(11) Loken, N.; Paddon-Row: M. N.; Smith, T. A.; La Rosa, M.; Ghiggino, K. P. *J. Am. Chem. Soc.* **1999**, *121*, 2917.
(12) Head, N. J.; Thomas, J.; Shephard, M. J.; Paddon-Row: M. N.; Bell, T. D.; Cabral, N. M.; Ghiggino, K. P. *J. Photochem. Photobiol. A: Chem.* **2000**, *133*, 105.
(13) Forster, R. J.; Keyes, T. E.; Majda, M. *J. Phys. Chem. B* **2000**, *104*, 4425.
(14) Forster, R. J.; Loughman, P. J.; Keyes, T. E. *J. Am. Chem. Soc.* **2000**, *122*, 11948.
(15) Imahori, H.; Tamaki, K.; Guldi, D. M.; Luo, C.; Fijitsuka, M.; Ito, O.; Sakata, Y.; Fukuzumi, S. *J. Am. Chem. Soc.* **2001**, *123*, 2607. Bell, T. D. M.; Ghiggno, K. P.; Jolliffe, K. A.; Ranasinghe, M. G.; Langford, S. J.; Shephard, M. J.; Paddon-Row, M. N. *J. Phys. Chem. A* **2002**, *106*, 10079.

(16) (a) Paddon-Row, M. N. *Adv. Phys. Org. Chem.* **2003**, *38*, 1. (b) Paddon-Row, M. N. *Aust. J. Chem.* **2003**, *56*, 729. (c) Paddon-Row, M. N. In *Electron-Transfer In Chemistry*; Balzani, V., Ed.; Wiley-VCH: Weinheim, Germany, 2001; Vol. 3, Part 2, Chapter 1, p 179.

(17) van der Boom, T.; Hayes, R. T.; Zhao, Y.; Bushard, P. J.; Weiss, E. A.; Wasielewski, M. R. *J. Am. Chem. Soc.* **2002**, *124*, 9582.

(18) Davis, W. B.; Ratner, M. A.; Wasielewski, M. R. *Chem. Phys.* **2002**, *281*, 333.

(19) Shaakov, S.; Galili, T.; Stavitski, E.; Levanon, H.; Lukas, A.; Wasielewski, M. R. *J. Phys. Chem. A* **2003**, *125*, 6563.

(20) Heinen, U.; Berthold, T.; Kothe, G.; Stavitski, E.; Galili, T.; Levanon, H.; Wiederrecht, G.; Wasielewski, M. R. *J. Phys. Chem. A* **2002**, *106*, 1933.

(21) Blank, A.; Galili, T.; Levanon, H. *J. Porphyrins Phthalocyanines* **2001**, *5*, 58.

(22) Berg, A.; Shuali, Z.; Asano-Someda, M.; Levanon, H.; Fuhs, M.; Möbius, K. *J. Am. Chem. Soc.* **1999**, *121*, 7433.

(23) Levanon, H. *RIKEN Rev.* **1999**, *24*, 38.

(24) Asano-Someda, M.; Levanon, H.; Sessler, J. L.; Wang, R. *Mol. Phys.* **1998**, *95*, 935.

(25) Wasielewski, M. R.; Niemczyk, M. P.; Svec, W. A.; Pewitt, E. B. *J. Am. Chem. Soc.* **1985**, *107*, 1080. Wasielewski, M. R.; Niemczyk, M. P.; Svec, W. A.; Pewitt, E. B. *J. Am. Chem. Soc.* **1985**, *107*, 5562.

(26) Gust, D.; Moore, T. A. In *Advances in Photochemistry*; Volman, D. H., Hammond, G. S., Neckers, D. C., Eds.; Wiley: New York, 1991; p1.

(27) Sumi, H.; Marcus, R. A. *J. Chem. Phys.* **1986**, *84*, 4894.

(28) Miller, J. R.; Calcaterra, L. T.; Closs, G. L. *J. Am. Chem. Soc.* **1984**, *106*, 3047.

(29) Closs, G. L.; Johnson, M. D.; Miller, J. R.; Piotrowiack, P. *J. Am. Chem. Soc.* **1989**, *111*, 3751.

(30) Closs, G. L.; Miller, J. R. *Science* **1988**, *240*, 440.

(31) Zelent, B.; Messier, P.; Gauthier, S.; Gravel, D.; Durocher, G. *J. Photochem. Photobiol. A*: *Chem.* **1990**, *52*, 165.

(32) Gravel, D.; Gauthier, S.; Brissa, F.; Raymond, S.; D'Amboise, M.; Messier, P.; Zelent, B.; Durocher, G. *Can. J. Chem.* **1990**, *68*, 908.

(33) Zelent, B.; Ganguly, T.; Farmer, L.; Gravel, D.; Durocher, G. *J. Photochem. Photobiol. A*: *Chem.* **1991**, *56*, 165.

(34) Ganguly, T.; Farmer, L.; Gravel, D.; Durocher, G. *J. Photochem. Photobiol. A*: *Chem.* **1991**, *60*, 63.

(35) Okura, I.; Hosono, H. *J. Phys. Chem.* **1992**, *96*, 4466.

(36) Helsen, N.; Viaene, L.; Van der Auweraer, M.; De Schryver, F. C. *J. Phys. Chem.* **1994**, *98*, 1532.

(37) Bolton, J. R.; Schmidt, J. A.; Ho, T.; Liu, J.; Roach, K. J.; Weedon, A. C.; Archer, M. D.; Wilford, J. H.; Gadzekpo V. P. Y. *Electron transfer in Inorganic, Organic and Biological systems*; Bolton, J. R., Mataga, N., McLendon, G. L., Eds.; Adv. Chem. Ser. No. 228; American Chemical Society: Washington, DC, 1991; p 117.

(38) Misra, T.; Bhattacharya, T.; Pal, S. K.; De, A.; Saini, R. D.; Ganguly, T. *Chem. Phys. Lett.* **2003**, *382*, 167.

(39) Potter, C. A. S.; Brown, R. G.; Volmer, F.; Rettig, W. *J. Chem. Soc., Faraday Trans.* **1994**, *90*, 59.

(40) Gaplovsky, A.; Toma, T.; Luche, J.; Jakubikova, B.; Gaplovska, K.; Mranova, R. *J. Chem. Soc., Perkin Trans.* **2002**, *2*, 652.

(41) Maiti, M.; Misra, T.; Sinha, S.; Pal, S. K.; Mukherjee, D.; Saini, R. D.; Ganguly, T. *J. Luminesc.* **2001**, *93*, 261.

(42) Jana, P.; Mallik, P. K.; Ganguly, T.; Banerjee, S. B. *J. Luminesc.* **1990**, *46*, 235.

(43) Chatterjee, K.; Laha, S.; Chakravorti, S.; Ganguly, T.; Banerjee, S. B. *Can. J. Chem.* **1984**, *62*, 1369.

(44) Ganguly, T.; Farmer, L.; Li, W.; Bergeron, J. Y.; Gravel, D.; Durocher, G. *Macromolecules* **1993**, *26*, 2315.

(45) Jana, P.; De, R.; Ganguly, T. *J. Luminesc.* **1994**, *59*, 1.

(46) (a) Becke, A. D. *J. Chem. Phys.* **1993**, 98, 5648. (b) Lee, C.; Yang, W.; Parr, R. G. *Phys. Rev. B* **1988**, *37*, 785. For reviews of density-functional methods see: (c) Ziegler, T. *Chem. Rev.* **1991**, *91*, 651. (d) *Density Functional Methods in Chemistry*; Labanowski, J., Andzelm, J., Eds.; Springer: Berlin, Germany, 1991. (e) Parr, R. G.; Yang, W. *Density-Functional Theory of Atoms and Molecules*; Oxford University Press: New York, 1989. (f) Koch, W.; Holthausen, M. C. *A Chemist's Guide to Density Functional Theory;* Wiley-VCH: Weinheim, Germany, 2000.

(47) Hehre, W. J.; Radom, L.; Pople, J. A.; Schleyer, P. V. R. *Ab Initio Molecular Orbital Theory*; John Wiley & Sons: New York, 1986.

(48) Hanson, L. K.; Fajer, J.; Thompson, L. A.; Zerner, M. C. *J. Am. Chem. Soc.* **1987**, *109*, 4728.

(49) (a) Bacon, A. D.; Zerner, M. C. *Theor. Chim. Acta* **1979**, *53*, 21. (b) Anderson, P.; Edwards, W. D.; Zerner, M. C. *Inorg. Chem.* **1986**, *25*, 2728. (c) Zerner, M. C.; Lowe, G. H.; Kirchner, R. F.; Mueller-Westerhoff, U. T. *J. Am. Chem. Soc.* **1980**, *102*, 589. (d) Ridley, E.; Zerner, M. C. *Theor. Chim. Acta* **1973**, *32*, 111. (e) Ridley, J. E.; Zerner, M. C. *Theor. Chim. Acta* **1976**, 42, 223. (f) Thompson, M. A.; Zerner, M. C. *J. Am. Chem. Soc.* **1991**, *113*, 8210. (g) Zerner, M. C. in *Reviews in Computational Chemistry*; Lipkowitz, K. B., Boyd, D. B., Eds.; VCH Publishing: New York, 1991; Vol. 2, pp 313−366. (h) Zerner, M. C.; Correa de Mello, P.; Hehenberger, M. *Int. J. Quantum Chem.* **1982** *21*, 251.

(50) Adamo, C.; Scuseria, G. E.; Barone, V. *J. Chem. Phys.* **1999**, *111*, 2889.

(51) (a) Bauernschmitt, R.; Ahlrichs, R. *Chem. Phys. Lett.* **1996**, *256*, 454. (b) Bauernschmitt, R.; Hser, M.; Treutler, O.; Ahlrichs, R. *Chem. Phys. Lett.* **1997**, *264*, 573. (c) Wiberg, K. B.; Stratmann, R. E.; Frisch, M. J. *Chem. Phys. Lett.* **1998**, *297*, 60. (d) Handy, N. C.; Tozer, D. J. *J. Comput. Chem.* **1999**, *20*, 106. (e) Hirata, S.; Head-Gordon, M. *Chem. Phys. Lett.* **1999**, *302*, 375.

(52) (a) Cammi, R.; Mennucci, B.; Tomasi, J. *J. Phys. Chem. A* **2000**, *104*, 5631. (b) Cossi, M.; Barone, V. *J. Chem. Phys.* **2000**, *112*, 2427. (c) Cossi, M.; Barone, V. *J. Chem. Phys.* **2001**, *115*, 4708.

(53) Frisch, M. J.; Trucks, G. W.; Schlegel, H. B.; Scuseria, G. E.; Robb, M. A.; Cheeseman, J. R.; Zakrzewski, V. G.; Montgomery, J. A., Jr.; Stratmann, R. E.; Burant, J. C.; Dapprich, S.; Millam, J. M.; Daniels, A. D.; Kudin, K. N.; Strain, M. C.; Farkas, O.; Tomasi, J.; Barone, V.; Cossi, M.; Cammi, R.; Mennucci, B.; Pomelli, C.; Adamo, C.; Clifford, S.; Ochterski, J.; Petersson, G. A.; Ayala, P. Y.; Cui, Q.; Morokuma, K.; Malick, D. K.; Rabuck, A. D.; Raghavachari, K.; Foresman, J. B.; Cioslowski, J.; Ortiz, J. V.; Baboul, A. G.; Stefanov, B. B.; Liu, G.; Liashenko, A.; Piskorz, P.; Komaromi, I.; Gomperts, R.; Martin, R. L.; Fox, D. J.; Keith, T.; Al-Laham, M. A.; Peng, C. Y.; Nanayakkara, A.; Gonzalez, C.; Challacombe, M.; Gill, P. M. W.; Johnson, B.; Chen, W.; Wong, M. W.; Andres, J. L.; Gonzalez, C.; Head-Gordon, M.; Replogle, E. S.; Pople, J. A. *Gaussian 98*; Gaussian Inc.: Pittsburgh, PA.

(54) Frisch, M. J.; Trucks, G. W.; Schlegel, H. B.; Scuseria, G. E.; Robb, M. A.; Cheeseman, J. R.; Montgomery, J. A., Jr.; Vreven, T.; Kudin, K. N.; Burant, J. C.; Millam, J. M.; Iyengar, S. S.; Tomasi, J.; Barone, V.; Mennucci, B.; Cossi, M.; Scalmani, G.; Rega, N.; Petersson, G. A.; Nakatsuji, H.; Hada, M.; Ehara, M.; Toyota, K.; Fukuda, R.; Hasegawa, J.; Ishida, M.; Nakajima, T.; Honda, Y.; Kitao, O.; Nakai, H.; Klene, M.; Li, X.; Knox, J. E.; Hratchian, H. P.; Cross, J. B.; Adamo, C.; Jaramillo, J.; Gomperts, R.; Stratmann, R. E.; Yazyev, O.; Austin, A. J.; Cammi, R.; Pomelli, C.; Ochterski, J. W.; Ayala, P. Y.; Morokuma, K.; Voth, G. A.; Salvador, P.; Dannenberg, J. J.; Zakrzewski, V. G.; Dapprich, S.; Daniels, A. D.; Strain, M. C.; Farkas, O.; Malick, D. K.; Rabuck, A. D.; Raghavachari, K.; Foresman, J. B.; Ortiz, J. V.; Cui, Q.; Baboul, A. G.; Clifford, S.; Cioslowski, J.; Stefanov, B. B.; Liu, G.; Liashenko, A.; Piskorz, P.; Komaromi, I.; Martin, R. L.; Fox, D. J.; Keith, T.; Al-Laham, M. A.; Peng, C. Y.; Nanayakkara, A.; Challacombe, M.; Gill, P. M. W.; Johnson, B.; Chen, W.; Wong, M. W.; Gonzalez, C.; Pople, J. A. *Gaussian 03*; Gaussian, Inc., Pittsburgh, PA, 2003.

(55) Misra, T.; Ganguly, T.; Kamila, S.; Basu, C.; De, A. *Spectrochim. Acta A* **2001**, *57*, 2795.

(56) Manring, L. E.; Gu, C. H.; Foote, C. S. *J. Phys. Chem.* **1983**, *87*, 40.

(57) Isakasson, M.; Kalinin, S.; Lobov, S.; Ny, T.; Johansson, L. B. A. *J. Fluoresc.* **2003**, *13*, 379.

(58) Mulliken, R. S.; Rieke, C. A. *Phys. Soc. Rep. Prog. Phys.* **1941**, *8*, 231.

(59) Turro, N. J. *Modern Molecular Photochemistry*; Benjamin: Menlo Park, CA, 1978; Chapter 6.

(60) Kikuchi, K. *J. Photochem. Photobiol. A*: *Chem.* **1992**, *65*, 149.

(61) Chatterjee, K.; Laha, S.; Chakravorti, S.; Ganguly, T.; Banerjee, S. B. *J. Chem. Soc., Parkin Trans. 2* **1986**, 79.

(62) Zimmermann, C.; Mohr, M.; Zipse, H.; Eichberger, R.; Schnabel, W. *J. Photochem. Photobiol. A*: *Chem.* **1999**, *125*, 47.

(63) Ikegami, M.; Arai, T. *J. Chem. Soc., Perkin Trans.* **2002**, *2*, 342.